Cytoplasmic pH and Human Erythrocyte Shape

Margaret M. Gedde, Debra K. Davis, and Wray H. Huestis
Department of Chemistry, Stanford University, Stanford, California 94305 USA

ABSTRACT Altered external pH transforms human erythrocytes from discocytes to stomatocytes (low pH) or echinocytes (high pH). The mechanism of this transformation is unknown. The preceding companion study (Gedde and Huestis) demonstrated that these shape changes are not mediated by changes in membrane potential, as has been reported. The aim of this study was to identify the physiological properties that mediate this shape change. Red cells were placed in a wide range of physiological states by manipulation of buffer pH, chloride concentration, and osmolality. Morphology and four potential predictor properties (cell pH, membrane potential, cell water, and cell chloride concentration) were assayed. Analysis of the data set by stratification and nonlinear multivariate modeling showed that change in neither cell water nor cell chloride altered the morphology of normal pH cells. In contrast, change in cell pH caused shape change in normal-range membrane potential and cell water cells. The results show that change in cytoplasmic pH is both necessary and sufficient for the shape changes of human erythrocytes equilibrated in altered pH environments.

INTRODUCTION

Human erythrocytes equilibrated in altered pH buffers at room temperature assume altered shapes. Below external pH 6.0, membrane curvature becomes negative (stomatocytic); above pH 8.0, curvature becomes positive (echinocytic) (Gedde and Huestis, 1997). This phenomenon appears to be related to the pH-dependent shape changes of red cells in electrical fields (Rand et al., 1965) and red cells exposed to glass (Furchgott and Ponder, 1940; Bessis and Prenant, 1972; Weed and Chailley, 1973). These shape changes have distinctive common features: 1) they proceed at ambient temperature; 2) they can occur within seconds; and 3) they reverse upon normalization of the extracellular environment (Rand et al., 1965; Bessis and Prenant, 1972; Weed and Chailley, 1973; Gedde and Huestis, 1997). Taken together, these features suggest that the shape changes result from changes in weak, noncovalent bonds, rather than higher energy bonds. Because the plasma membrane determines red cell shape, the events that produce altered shape presumably take place in the red cell membrane. Expansion and contraction of the spectrin membrane skeleton upon change in cell pH are expected to strongly affect membrane curvature (Elgsaeter et al., 1986), but predicted curvature changes are in the direction opposite those observed in intact cells.

Study of the molecular basis of this shape change has been hampered by uncertainty about the identity of the mediating red cell physiological property. The previous paper (Gedde and Huestis, 1997) showed that membrane potential, which has been reported to be the mediating property, does not predict red cell shape. To identify which of three other cell properties (cell pH, cell chloride, and cell water) correlate with observed shape changes, conditions were sought to vary them independently. Stratification and multivariate modeling were used to isolate the effects of each variable. This paper presents data identifying the mediating physiological property as cell pH.

MATERIALS AND METHODS

Buffering compounds and nystatin were purchased from Sigma (St. Louis, MO). Other chemicals were reagent grade. Red cells and solutions were prepared as described (Gedde and Huestis, 1997). Cell properties were assayed as described (Gedde and Huestis, 1997).

Buffer specifications predicted to vary cell pH, cell water, and membrane potential independently

The equations of red cell physiology (Jacobs and Stewart, 1947; Freedman and Hoffman, 1979) were used to calculate specifications for buffers predicted to produce targeted cell states. Cell states were defined by cell pH (pH_{in}), membrane potential ($\Delta\Psi$), and cell water (cw). Results specified buffer pH (pH_{out}), chloride concentration ($[Cl]_{out}$), and osmolality (Os_{out}).

Buffer pH was calculated from cell pH and membrane potential:

$$pH_{out} = pH_{in} - (\Delta\Psi/59). \quad (1)$$

To determine buffer Cl concentration, total cell chloride (Cl_{tot}) in femtomoles was determined as a function of cell pH (Gedde and Huestis, 1997) and expressed as two linear functions:

$$\text{For } pH_{in} < 7.9: \quad Cl_{tot} = 50.2 - 6.10\, pH_{in} \quad (2a)$$

$$\text{For } pH_{in} \geq 7.9: \quad Cl_{tot} = 12.8 - 1.35\, pH_{in}. \quad (2b)$$

Received for publication 28 September 1994 and in final form 3 December 1996.

Address reprint requests to Dr. Wray H. Huestis, Department of Chemistry, Stanford University, Stanford, CA 94305. Tel.: 415-723-2503; Fax: 415-723-4817; E-mail: hf.whu@forsythe.stanford.edu.

Dr. Gedde's present address is Department of Pathology and Laboratory Medicine, Hospital of the University of Pennsylvania, Philadelphia, PA 19104.

Dr. Davis's present address is Oregon Health Sciences University, Portland, OR 97201.

0006-3495/97/03/1234/13 $2.00

Then $[Cl]_{in}$ (molal) = Cl_{tot} (fmol)/cw (pg). Cell chloride activity coefficients (γ_{Cl}) were calculated as a function of chloride concentration (Gedde and Huestis, 1997, Appendix A). Then with $[Cl]_{out} = (a_{Cl})_{out}/(\gamma_{Cl})_{out}$ and

$$(a_{Cl})_{out} = \left(\frac{(a_{Cl})_{in}}{e^{(\Delta\Psi/25.5)}}\right), \quad (3)$$

$[Cl]_{out}$ was calculated by iteration.

Buffer osmolality was determined from cell water and cell osmoles (O_c). Cell osmoles was found as a function of cell pH and cell water. This expression was determined as follows: cell osmoles were measured at a range of cell pHs. For each sample, hemoglobin osmoles was calculated as a function of cell water (Gedde and Huestis, 1997, Appendix B) and subtracted from cell osmoles. The adjusted cell osmole values then were plotted and fit as a function of cell pH. To the fitted expression, hemoglobin osmoles were added again as a function of cell water, yielding an expression for total cell osmoles:

$$O_c(\text{fosmol}) = 60.4 - 8.05\ pH_{in} + 0.295\ pH_{in}^2 + \left(\frac{16.8}{cw}\right) + \left(\frac{3440}{cw^2}\right). \quad (4)$$

Then buffer osmolality (Os_{out}) was calculated from $Os_{out} = O_c/cw$.

These calculations assumed constant cell cation content. Therefore their applicability was limited by leakage of cell salts in low-chloride solutions (see Results).

Nystatin treatment

A nystatin stock solution of 25 mg/ml was prepared in dimethyl sulfoxide (DMSO) on the day of each experiment. Stock was added to experimental solutions in glass vessels at the temperature of the experiment to give a final concentration of 50 μg/ml (final DMSO concentration, 0.2%).

To assess the effect of nystatin treatment on shape at normal ionic strength, solutions and cells were chilled to 4°C. Cells were resuspended at 10% in 120 mM KCl and 45 mM sucrose containing nystatin, and incubated on ice for 10 min. They were washed twice in the same solution with nystatin, then once without nystatin, all at 4°C. After four more washes at room temperature in the same solution without nystatin, cells were resuspended in 120 mM KCl, 15 mM sucrose, and 20 mM HEPES at pH 7.4, and morphology was assayed after 10 min.

The same protocol was followed to elevate cell potassium chloride, except that, after the initial nystatin incubation in 120 mM KCl/sucrose, samples were washed in 300 mM KCl/sucrose and were resuspended in 300 mM KCl/sucrose/HEPES. To reduce cell salt, cells were resuspended at 1% Hct and 4°C in 150 mM KCl and 45 mM sucrose containing nystatin, and incubated for 10 min. (The dilute suspension prevented the membrane vesiculation that occurred at 10% Hct.) The cells were then washed at 4°C once in 10 mM KCl and 150 mM sucrose containing nystatin, and once in 10 mM KCl and 45 mM sucrose containing nystatin. (The intermediate osmolality of the 150 mM sucrose solution was necessary to prevent large, potentially lytic variations in cell water content.) Cells were washed once at 4°C and twice at room temperature in 10 mM KCl and 45 mM sucrose without nystatin, then resuspended at 10% in 10 mM KCl, 15 mM sucrose, and 20 mM HEPES (pH 7.4). Morphology was assayed after 10 min.

These protocols prevented the large variations in cell water content (swelling or shrinkage) that can occur upon permeabilization of cells to cations.

Depletion of cell potassium chloride in low external chloride solution

Cells were washed and resuspended at 1% Hct in 270 mM sucrose or at 10% Hct in 250 mM sucrose and 10 mM KCl, and incubated at 37°C for 15–60 min. This depleted total cell chloride to 20–50% of original levels. The chloride-depleted cells were resuspended at 10% Hct in approximately 150 mosm KCl-sucrose solutions buffered at neutral pH by 20 mM citrate or HEPES. In some samples, up to 200 mM ammonium chloride was added to the final equilibrating buffer. The ammonium cation, through its equilibrium with permeant ammonia, provided a permeant counterion to accompany chloride into cells, allowing elevation of cell chloride to up to 300 mM. After equilibration, morphology was assayed.

Mathematical modeling of shape as a function of three cell properties

Nonlinear multivariate modeling was performed using RS/Explore (BBN Software Products Corporation, Cambridge, MA). Modeling proceeded in three phases: 1) choice of appropriate mathematical terms, 2) application of a fitting protocol, and 3) identification of outliers.

Choice of the mathematical form of the model

Stratification of the data set showed that cell pH had an independent, strongly nonlinear effect on shape (Results). In preliminary curve fitting, a cubic equation best approximated the dependence. In contrast, stratification showed that membrane potential and cell water had no independent effect on shape. Consistent with these results, independent terms containing cell pH to third order (pH, pH^2, and pH^3), but no independent membrane potential or cell water terms, were added to the model. To model possible effects on the shape of interactions of membrane potential and cell water with the primary predictor cell pH, interaction terms containing membrane potential or cell water and cell pH (pH*pot, pH^2*pot, pH3*pot, pH*cw, pH^2*cw, and pH^3*cw, where pot = potential and cw = cell water) were added to the model. The stratification results suggested no other appropriate terms. With the intercept, this gave an initial 10-term mathematical model to be fit to the 94 data points.

In the initial definition of model variables, the origins of the cell pH and cell water variables were made equal to their normal values, 7.2 and 67 pg, respectively (i.e., model cell pH = [actual cell pH − 7.2], and model cell water = [actual cell water − 67]). This step improved the orthogonality of the final fitted model.

Fitting of the model to the data set

Multiple least-squares regression was used to calculate initial coefficients for the 10-term model. Variance in the initial model was strongly pH-dependent (consistent with Fig. 1); thus the basic statistical assumption of constant variance of response across predictor variables did not hold. Accordingly, pH-dependent variance-adjustment weights, which weighted

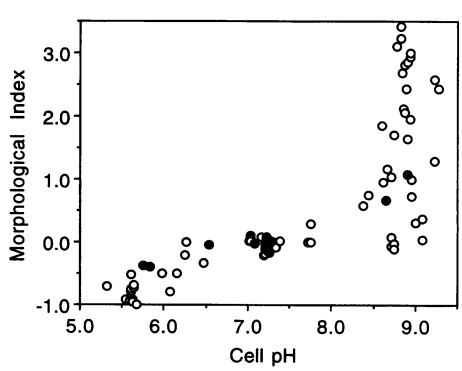

FIGURE 1 Graphical correlation of morphology with cell pH. Correlation of morphology with cell pH in the full data set (94 cases). ●, Cases with normal range membrane potential (−15 to +15 mV) and cell water (63 to 72 pg).

each observation inversely proportionally to its group's estimated variance, were incorporated into the model. In addition, robust fitting, which prevents outliers from unduly influencing fit in outlier-prone data, was shown to give improved fit of this data set. Accordingly, the fitting regression procedure was changed from least squares to robust bisquare. In a stepwise regression protocol, the term pH^3*cw was determined not to contribute significantly to the fit of the model ($p > 0.05$) and was removed.

Identification of outliers

Consistent with the analytical observation that the data set was outlier-prone, five of the 94 cases were found to have residuals lying outside the range expected for independent, normally distributed errors (threshold = 0.5) and were therefore identified as outliers. The physiological states of these samples were 1) low pH, swollen, positive potential; 2) high pH, shrunken, negative potential; 3) high pH, shrunken, neutral potential; 4) high pH, shrunken, positive potential; and 5) high pH, normal cell water, positive potential. In the first four of these samples, the observed morphological index was low relative to that predicted by the fitted model; in the last, the observed morphological index was high.

To minimize variability in the mathematical model, making it maximally useful for quantitative testing of hypotheses, the five outlier cases were excluded. The model was refit to the remaining 89 cases.

Prediction of morphological index

The fitted model was used to calculate predicted morphologies for specific cell states defined by cell pH, membrane potential, and cell water. Simultaneous confidence intervals (67%) were calculated for each predicted morphology. The significance of differences between predicted values was determined by the two-sided *t*-test.

Adjusted-MI plots

The fitted model was used to calculate three adjusted-MI plots, one for each predictor. Adjusted-*y* plots display the response variable as a function of one predictor after adjusting for effects of the other predictors. Represent the fitted model equation as

$$MI_i = F(pH_i, pot_i, cw_i) + e_i,$$

where *i*'s are the 89 cases in the fitted model; the response is the morphological index; the predictors are cell pH, membrane potential, and cell water, respectively; and e_i's are the residuals for each case (that is, e_i = observed MI_i − predicted MI_i). Then the adjusted-fit function over the range of cell pH is defined as

$$\text{Adjusted MI (pH)} = \frac{1}{89}\sum_i F(pH, pot_i, cw_i).$$

This function was determined by calculating adjusted MI at 0.1 pH unit intervals over the range 5.3–9.3. In each calculation, a predicted MI was determined for each of the 89 cases by substituting the cell pH of interest and the actual membrane potential and cell water values for that case. These 89 predicted values were averaged, yielding the adjusted MI value at the specific cell pH. The plotted calculated values yielded the smooth curve shown in Fig. 5 *A*. Adjusted MIs were determined for each case by adding the residual of each case to the value of the adjusted MI function at the corresponding cell pH. These case-adjusted MIs are shown with the adjusted MI function in Fig. 5 *A*. Adjusted MIs as functions of membrane potential and of cell water were determined similarly (Fig. 5, *B* and *C*).

RESULTS

The aim of the present study was to identify which physiological properties mediate the shape change observed in altered pH solutions. Using several strategies, red cells were placed in a wide range of physiological states. Morphology and four physiological properties (cell pH, membrane potential, cell water, and cell chloride concentration) were assayed in each state. Morphology and the four parameters were correlated by a multivariate analysis sequence that included stratification and mathematical modeling. The results showed altered cell pH to be necessary and sufficient for discocyte-stomatocyte and discocyte-echinocyte transitions in altered pH solutions.

Choice of predictor physiological properties

External solution properties seemed unlikely to be primary predictors of morphology. Theoretically, external pH variation could affect membrane curvature by titrating and thereby altering the packing of the cell surface glycocalyx; however, the cell surface isoelectric point is dominated by strongly acidic sialic acid residues (pK about 2), and only minor change in surface charge occurs as the external pH varies between 5 and 10 (Glaser, 1979). External ionic strength has been shown to affect red cell membrane structure (Herrmann and Muller, 1986), but variation in external ionic strength does not perturb intact cell shape (Gedde and Huestis, 1997).

In the present study, three cell properties and one transmembrane property were hypothesized to predict red cell shape. Cell pH and cell water were chosen because preliminary data indicated that both had roles in determining shape. Membrane potential was chosen because it has been reported to affect shape. Cell chloride concentration was chosen as a marker for cell ionic strength, variation of which might affect shape by causing expansion or contraction of the membrane skeleton (Elgsaeter et al., 1986). (However, cell chloride concentration may be a suboptimal marker for ionic strength in the concentrated polyelectrolyte environment of the red cell cytoplasm.)

Previously examined cell states

Data from two types of experiments reported in the companion paper became the first cases in the data set assembled for this study. The first experiment varied external pH at constant external chloride and osmolality. This protocol caused simultaneous variation of morphology and the four physiological properties (Gedde and Huestis, figures 1 and 5). A total of 16 cases from three experiments were used.

The second experiment varied external chloride in unbuffered solutions, to vary membrane potential independently of cell pH, cell water, and cell chloride (Gedde and Huestis, figure 8). A total of 33 cases from seven experiments were accepted into the data set. Five of these experiments were those shown in the figure. A sixth was a chloride series in

which cell water varied because of cell salt leakage (see below); the final experiment was a chloride series at low cell pH. Two of these seven experiments used cells with elevated 2,3-diphosphoglycerate (2,3-DPG) levels. Additional cellular 2,3-DPG is expected to contribute significantly to cell ionic strength, making measured cell chloride concentration a less accurate reflection of cell ionic strength in cells with elevated 2,3-DPG than in untreated cells.

Targeted cell states

Independent shape effects of membrane potential had already been investigated. To investigate independent effects of cell pH, cell water, and cell chloride, conditions in which each of these parameters varied through low, normal, and high ranges while the other properties remained normal were targeted. To investigate possible interactive effects of these properties (for example, a synergistic effect of high cell pH and negative membrane potential), cell states with more than one altered property were also targeted. Target low, normal, and high values for each property were identified. These were cell pH, 5.5, 7.2, and 8.9 pH units; cell water, 55, 67, and 90 pg; membrane potential, −40, 0, and +40 mV; and cell chloride concentration, 10, 90, and 300 mM.

The two major methods used to approach targeted cell states were buffer variation and cell chloride variation. In the buffer variation method, cells were equilibrated in solutions of external pH, chloride, and osmolality calculated to produce specific cell pH, membrane potential, and cell water values. However, because cell chloride could not be specified independently of cell pH, investigation of cell chloride effects by this approach was limited. In the cell chloride variation method, cell chloride was set independently of cell pH through permeabilization of cells to positive counterions. However, permeabilization procedures themselves affected cell shape. The two approaches and these limitations are detailed below.

Achievement of targeted cell states by buffer variation

At equilibrium, three red cell properties (cell pH, membrane potential, and cell water) are determined collectively by three properties of the external medium (external pH, chloride concentration, and osmolality), assuming that nonpermeant cell contents are constant (Jacobs and Stewart, 1947; Freedman and Hoffman, 1979). Known relationships of these six properties allow calculation of external conditions predicted to yield specific combinations of cell pH, membrane potential, and cell water (see Materials and Methods; also Freedman and Hoffman, 1979). Cell chloride concentration cannot be specified and covaries with cell pH.

Solution compositions predicted to produce 21 target combinations of the three specifiable properties (Table 1) were calculated as described in Materials and Methods.

TABLE 1 Buffer specifications predicted to produce desired cell states

Cell state			Buffer specifications		
Cell pH	Membrane potential (mV)	Cell water (pg)	Buffer pH	Buffer chloride	Buffer osmolality
7.2	−10	55	7.37	0.175	0.348
		67		0.137	0.279
		90		0.106	0.204
	+40	55	6.52	0.021	0.348
		67		0.016	0.279
		90		0.013	0.204
5.5	+5	55	5.42	0.242	0.481
		67		0.190	0.389
		90		0.148	0.285
	+40	55	4.82	0.053	0.481
		67		0.042	0.389
		90		0.033	0.285
8.9	0	55	8.90	0.014	0.246
		67		0.011	0.196
		90		0.009	0.141
	+40	55	8.22	0.003	0.246
		67		0.002	0.196
		90		0.002	0.141
	−40	55	9.58	0.077	0.246
		67		0.060	0.196
		90		0.046	0.141

Buffer specifications predicted to give targeted cell states were calculated as described in Materials and Methods. Note that leakage of cell salts in low external chloride limited attainment of some targeted cell states (see Results).

Buffers with these compositions were made using potassium chloride, potassium gluconate or sucrose, and 2-[*N*-morpholino]ethanesulfonic acid, HEPES, or 2-[*N*-cyclohexylamino]-ethanesulfonic acid as described (Gedde and Huestis, 1997). Cells were equilibrated in these experimental buffers, and morphology and cell properties were assayed (Gedde and Huestis, 1997).

This approach produced some but not all of the target states necessary to assess the primary morphological effects of each property. Cell water was varied at normal cell pH, membrane potential, and cell chloride (the first three conditions in Table 1). Cell pH was varied at normal cell water and membrane potential, with covariation of cell chloride. Cell chloride concentration could not be varied significantly at normal cell pH, cell water, and membrane potential. (Cells with elevated 2,3-DPG can have low cell chloride concentration at normal cell pH, membrane potential, and cell water, but cell ionic strength is not necessarily low.)

Possible synergistic effects of the three specifiable properties were investigated by producing combination target states. Not all combinations of these properties were physiologically accessible in normal cells. No buffer composition could produce cells with low cell pH and very negative membrane potential. (At cell pH below 6.8 (cell isoelectric point), nonpermeant cell electrolytes are positively charged. At the low cell pHs achieved here, the large net positive charge requires large amounts of cell chloride as counterion, and cell chloride concentration is high. To produce a neg-

ative membrane potential, external chloride concentration must be made greater than cell chloride concentration. Attempting to meet this requirement by placing cells in a high external chloride solution causes cell shrinkage, concentrating cell chloride even more, again putting the required chloride gradient out of reach. Attempts to calculate buffer specifications for this cell state gave paradoxical results (the osmotic contribution of specified buffer chloride exceeded specified buffer osmolality).) Access to negative potentials in normal pH cells was limited as well.

Application of the buffer variation method was also limited by the increase in membrane permeability to potassium that occurs in red cells in low chloride solutions (Donlon and Rothstein, 1969; Jones and Knauf, 1985; Bernhardt et al., 1984). In buffers containing very low external chloride (for example, the buffer calculated to produce high cell pH, positive potential, and increased cell water), cells lost enough potassium chloride to breach the assumption of constant total cell chloride. The practical consequence was that, especially in high pH cells, positive potentials could not be achieved by buffer variation. Remedies to this problem were investigated.

Leakage of cell salts in low-chloride solutions

The extent of cell salt (potassium chloride) leakage under conditions used in this study was assessed. Normal pH cells were placed in isotonic, lowered chloride solutions (external potassium chloride was replaced osmole for osmole with sucrose), and total cell chloride was calculated from cell chloride concentration and cell water. Lowering external chloride from 150 to 40 mM allowed leakage of nearly 20% of total cell chloride; a drop to 10 mM external chloride allowed release of 50%. Means to prevent cell salt leakage at low external chloride were sought.

Low chloride cell salt leakage has been reported to be membrane potential-dependent (Donlon and Rothstein, 1969), but other reports suggest that ionic strength itself is the factor triggering leakage (Bernhardt et al., 1984; Jones and Knauf, 1985). If the latter is so, very positive potentials should be achievable by supplementation of external ionic strength. The requirements for a supplementing salt were that it be nonpermeant, so that it would not affect membrane potential, and that it not buffer in the external pH range of interest.

Use of potassium gluconate to prevent leakage of cell salts in low chloride solutions

Potassium gluconate has been reported to restore red cell membrane potassium permeability to normal in low chloride solutions (Bernhardt et al., 1987). The gluconate ion is nonpermeant with pK_a about 4. When potassium chloride in low chloride buffers was replaced osmole for osmole with potassium gluconate, cell salt leakage from normal pH cells was reduced but not eliminated. In solutions containing gluconate and 20 mM chloride salt, about 3% of cell chloride was lost; at 10 mM extracellular chloride, 20% of cell chloride passed the membrane. Discoid morphology of normal pH cells was not perturbed by this degree of leakage. In experiments subsequent to this finding, potassium gluconate (instead of sucrose) was used to replace potassium chloride in low external chloride experiments at normal and high pH.

Results of the buffer variation strategy

A wide variation of cell pH, cell water, and membrane potential was achieved. In high-pH cells, cell chloride leakage prevented access to membrane potentials more positive than +25 mV. Except for this constraint, each of the 21 target states listed in Table 1 was approximated by one or more samples, to a total of 28 cases. An additional 17 samples fell between the conditions specified in Table 1. Nearly all of these were high cell pH samples that missed their target states because of cell salt leakage not preventable by potassium gluconate (20–30% loss of cell chloride).

Achievement of targeted cell states through variation of cell chloride

For cell chloride to vary, chloride ions must enter or exit the cell accompanied by a positive counterion. When cell chloride changes during cell pH change, the counterion is the proton. For cell chloride to vary independently of cell pH, a different permeant cation must participate.

Three methods for varying cell chloride independently of cell pH were tested. Potassium was the counterion in the first two, and ammonium was the counterion in the third. They were 1) incubation with the cation ionophore nystatin, which reversibly permeabilizes the membrane to sodium and potassium; 2) incubation in low chloride solutions, which induces passage of cellular potassium through the anion exchanger; and 3) incubation with ammonium chloride, which results in an influx of chloride accompanied by ammonium, which is effectively permeant (see Materials and Methods).

The first two methods, permeabilization of the membrane to potassium by nystatin or by low chloride incubation, independently affected cell morphology. Nystatin-treated cells were stomatocytic after return of membrane permeability to normal by washing, whether cell chloride was elevated, reduced, or unaltered (MI −0.20 to −0.50 relative to control cells). (Nystatin was also observed to affect shape while still in the membrane. In general, nystatin was echinocytogenic; at low ionic strength, crenation was frequently severe enough to cause membrane vesiculation.) Change in the nystatin removal protocol (in number and temperature of washes and composition of final buffer) did not normalize final cell shape. Cells depleted of 50% of cell chloride by incubation in low chloride solutions were also stomatocytic (final morphology, −0.60 MI units).

The third method, incubation with ammonium chloride, allowed elevation of cell chloride to 300 mM (normal, 90 mM). However, cell physiology could not be manipulated easily with a permeant chloride counterion; moreover, when ammonium chloride was present, red cells at extremes of cell pH were susceptible to lysis.

These methods did allow comparison of the morphologies of normal pH cells that had a range of cell chloride concentrations. Cells treated with nystatin to yield cell chloride concentrations of 10 mM, 100 mM, and 300 mM had normal discoid to mildly stomatocytic morphology (MI −0.4 to 0.0). Cells incubated in low chloride medium to give a cell chloride concentration of 40 mM were also mildly stomatocytic (MI −0.3 to 0.0). Equilibration in up to 200 mM ammonium chloride (cell chloride concentration, 300 mM) yielded discoid cells (MI −0.1 to 0.0). Thus wide variation of cell chloride at normal pH had no discernible effect on shape.

Results of strategies to vary cell chloride

Cell chloride concentration was varied independently by three methods. Low chloride incubation depleted cell chloride, ammonium chloride incubation elevated cell chloride, and nystatin treatment could deplete or elevate cell choride at normal cell pH, cell water, and membrane potential. Variation of chloride between 10 and 300 mM by these methods had no discernible effect on cell shape. Most data were offset by independent effects of the treatments on shape, so no samples were accepted into the data set.

The data set

The above procedures generated 16 cases from variation of external pH, 33 from variation of external chloride, and 45 from calculated buffer variation (including 17 cases that fell short of target states). In this 94-case data set, cell pH varied from 5.3 to 9.3, membrane potential from −50 to +50 mV, cell water from 40 to 99 pg, and cell chloride from 0.2 to 262 mM. Most target states shown in Table 1 were represented among these data. Some theoretically allowed positive potential states were not achieved because of cell salt leakage.

A general unlinking of cell pH and cell chloride variation was not achieved in this data set. However, three factors caused minor separation of their variation. First, variation of cell water diluted and concentrated total cell chloride, producing some variation of cell chloride concentration at constant cell pH. Second, cell salt leakage lowered cell chloride at constant cell pH. Thus there was an analytical advantage to accepting samples that had undergone leakage into the data set. Third, elevation of 2,3-DPG produced very low chloride in some normal cell pH samples.

Because multivariate analysis is most reliable when predictor variables in a data set vary independently (Hennekens and Buring, 1987), the independence of variation of each predictor was assessed. In a completely orthogonal data set, the linear correlation coefficient between each pair of predictor variables is zero. Correlation coefficients for each pair of predictors are shown (Table 2A). Coefficients involving cell water were all close to zero. Coefficients involving membrane potential were midrange. Cell pH and cell chloride concentration were strongly correlated (coefficient −0.87).

Table 2B details the dependence of cell chloride, membrane potential, and cell water on cell pH in this data set. Ranges of these variables at low, normal, and high cell pH are shown. Cell water varied over nearly its whole range at each pH level. Negative potentials were not accessible at low pH; still, cases explored broad potential ranges at each pH level. In contrast, cell chloride ranges at each pH level barely overlapped. This again reflects nonorthogonality of the data set with respect to cell chloride concentration.

Primary stratification: independent effects of four physiological properties

Analysis of the multivariate data set proceeded in two phases: 1) stratification and 2) mathematical modeling. In the initial stratification step, the data set was grouped according to values of the most influential variable. Such a grouping allows independent effects of other predictor variables to be examined with less interference (Hennekens and Buring, 1987). All indicators pointed to cell pH as the most influential variable in the data set: linear correlation of morphological index with cell pH was higher than with any other predictor (Table 2A); morphological index and cell pH were strongly correlated in a plot of the full data set, despite wide variation of other cell properties (Fig. 1); and none of the other properties correlated graphically with morphology (Fig. 2, *A1*, *B1*, and *C1*). Accordingly, a nor-

TABLE 2 Data set orthogonality

A: Covariance of predictor variables

	Cell pH	Potential	Cell water	Cell chloride	MI
Cell pH	1.00	−0.43	−0.24	−0.87	0.78
Potential		1.00	0.09	0.56	−0.48
Cell water			1.00	0.14	−0.33
Cell chloride				1.00	−0.69

B: Effect of cell pH on accessible ranges of the other predictors

	Cell pH range		
	Low pH (<6.20)	Normal pH (7.15–7.40)	High pH (>8.50)
Membrane potential (mV)	0 to +50	−39 to +48	−50 to +24
Cell water (pg)	59 to 99	41 to 83	40 to 98
Cell chloride (mM)	139 to 262	14 to 141	0.2 to 23

Part A shows linear correlation coefficients describing the degree of covariance among four independent variables and morphology in the 94-case data set.

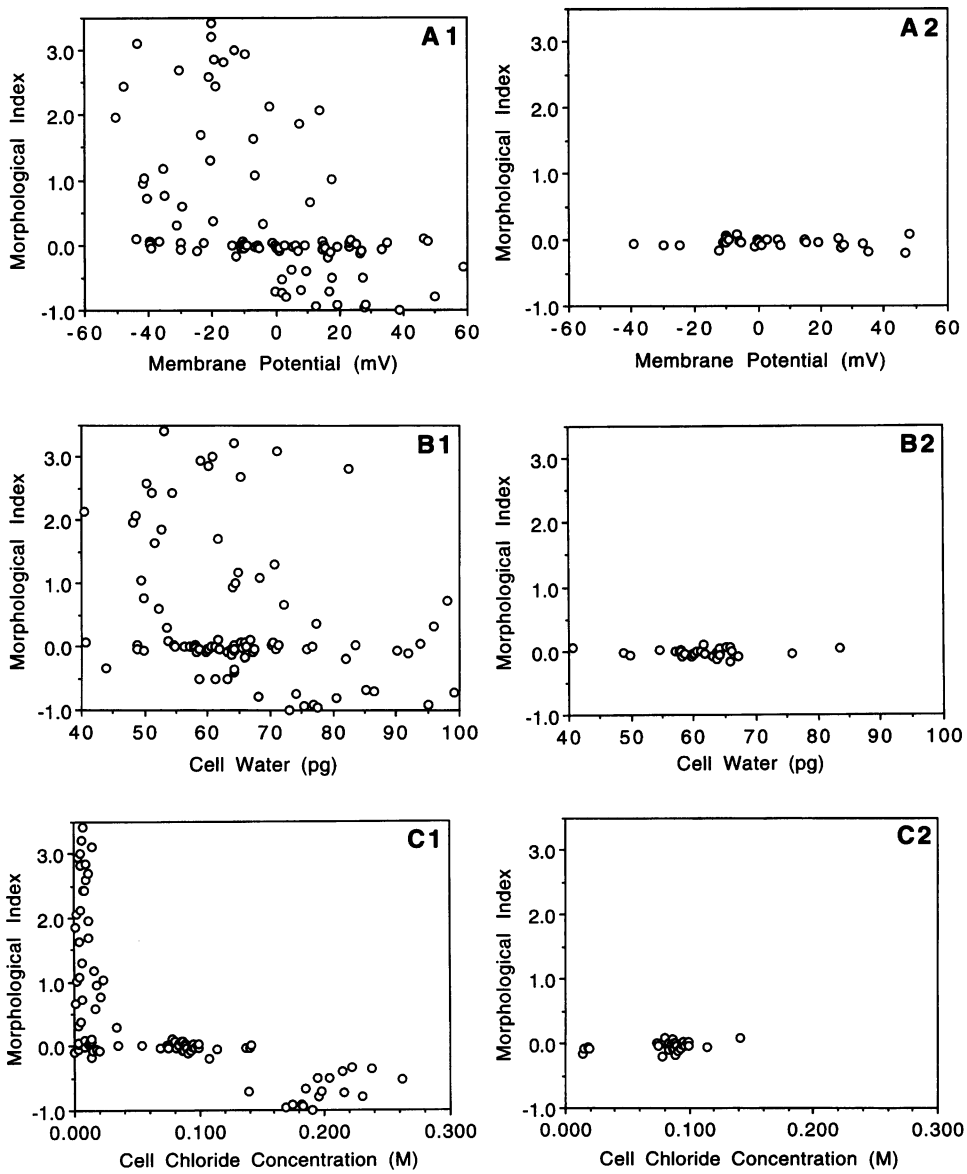

FIGURE 2 Graphical correlation of morphology with membrane potential, cell water, and cell chloride. Correlation between morphology and membrane potential (*A*), cell water (*B*), and cell chloride concentration (*C*) in 1) the full data set (94 cases, cell pH 5.32–9.28) and 2) the normal pH subset (29 cases, cell pH 7.15–7.40). Compare *A1*, *B1*, and *C1* to Fig. 1.

mal cell pH subset of 29 cases (cell pH 7.15–7.40) was identified.

The morphological index of each case in this normal cell pH subset was plotted as a function of each other predictor (Fig. 2). Membrane potential variation had no effect on shape in this subset (Fig. 2 *A2*), consistent with results in the companion study. Cell chloride variation within the normal cell pH subset had no effect on shape (Fig. 2 *B2*), also expected from results of experiments varying cell chloride. Cell water variation also had no shape effect at normal cell pH (Fig. 2 *C2*); this finding was unexpected (see Discussion).

To assess the independent effect of variation of cell pH, a set of 10 cases having the full range of cell pHs but a normal range of values of membrane potential and cell water (membrane potential −15 to +15 mV; cell water 63 to 72 pg) was identified. Within a normal range of membrane potential and cell water, morphology still varied from stomatocytic to echinocytic as cell pH varied from about 5.5 to 9.0 (Fig. 1, *filled symbols*).

Results of primary stratification

Cell pH independently affected erythrocyte shape; cell water, membrane potential, and cell chloride concentration did not independently affect shape. Thus in this system cell pH variation was necessary and sufficient for erythrocyte shape change.

Second-level stratification

The range of morphologies observed at low and high cell pH (Fig. 1) suggested that variation of other properties might exert secondary effects. Second-level stratification

was used to examine this possibility. The range of cell states in the data set allowed the consideration of two hypotheses.

The first hypothesis was that membrane potential influenced the degree of shape change observed at low or high pH. To separate effects of membrane potential changes from those of cell water, a normal cell water stratum was identified (63–72 pg, 32 cases). Within this stratum, three levels of membrane potential were identified; then morphological index was plotted against cell pH for each membrane potential level (Fig. 3 *A*). The plot suggested that echinocytosis in high pH cells might be modulated by membrane potential, with negative potentials producing more echinocytic cells.

The second hypothesis was that cell water influenced the degree of shape change observed at low or high cell pH. To examine effects of cell water changes separately from those of membrane potential, a normal membrane potential stratum was identified (−15 to +15 mV, 41 cases). Within this stratum, three levels of cell water were identified, and the morphological index was plotted against cell pH at each level of cell water (Fig. 4 *A*). This plot suggested that high cell pH echinocytosis might also be modulated by cell water, with shrinkage intensifying the echinocytosis and swelling relieving it.

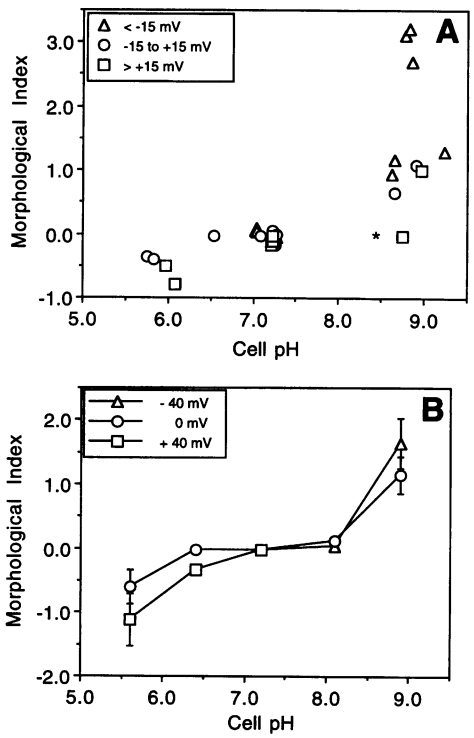

FIGURE 3 Secondary morphological effects of membrane potential: stratification and model predictions. (*A*) Morphological index of the normal cell water range subset (63–72 pg; 32 cases), plotted against cell pH for three membrane potential ranges (identified in the figure key). The asterisk identifies a case subsequently determined to be an outlier. (*B*) Morphological index predicted by the model for five values of cell pH and three values of membrane potential, at cell volume = 72 pg. Positive potentials were calculated only at low pH, and negative potentials only at high pH, to reflect the limitations of the experimental data set. Error bars represent 67% confidence intervals; for clarity, they are shown on the pH 5.6 and 8.9 points only.

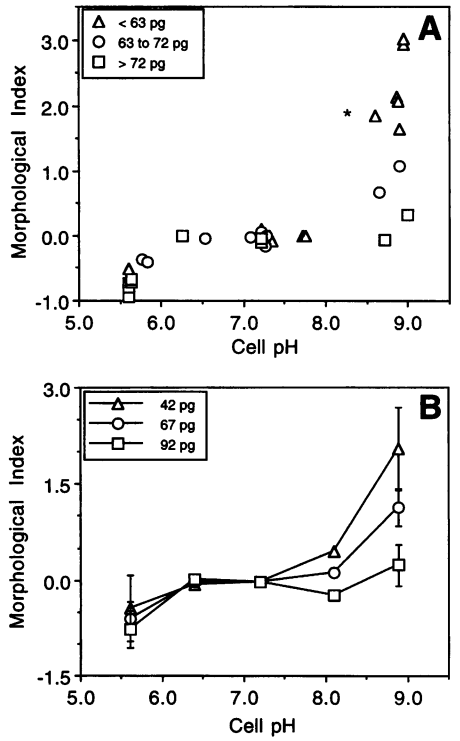

FIGURE 4 Secondary morphology effects of cell water: stratification and model predictions. (*A*) Morphological index of the normal membrane potential range subset (−15 to +15 mV, 41 cases), plotted against cell pH for three cell water ranges (identified in the figure key). The asterisk identifies a case subsequently determined to be an outlier. (*B*) Morphological index predicted by the model for five values of cell pH and three values of cell water, at membrane potential = 0 mV. Error bars represent 67% confidence intervals; for clarity, they are shown on the pH 5.6 and 8.9 points only.

Predictions of a mathematical model of morphology as a function of three physiological properties

Stratification demonstrated an independent effect of cell pH on morphology, as well as possible secondary effects of membrane potential and cell water on the shape of high pH cells. To examine these effects quantitatively, a mathematical model of morphological index as a function of cell pH, membrane potential, and cell water was constructed and fitted (see Materials and Methods). The model contained independent cell pH terms to third order. Inclusion of membrane potential–cell pH and cell water–cell pH interaction terms was found to significantly improve fit of the model to the data ($p < 0.05$), suggesting that apparent secondary effects of potential and cell water seen in the stratification steps were quantitatively significant. The fitted model was substantively orthogonal (condition number = 10) with a low RMS error (0.14 MI units). (The condition number of a perfectly orthogonal model is 1. Condition numbers of

models with significant covariance of variables can be greater than 10,000. Reasonably orthogonal models have condition numbers of less than 50 (BBN Software Products Corporation, 1988).) The final terms and their coefficients are shown in Table 3.

Morphologies predicted by the model were calculated for selected cell states and plotted with simultaneous confidence intervals (67%) (Figs. 3 *B* and 4 *B*). Consistent with stratification results, cell pH independently modulated shape: predicted morphologies of cells at pH 5.6 and 8.9, and with normal membrane potential and cell water, were significantly different ($p < 0.05$, two-tailed *t*-test; *open circles* in Figs. 3 *B* and 4 *B*). Visually, secondary effects of both membrane potential (Fig. 3 *B*) and cell water (Fig. 4 *B*) also appeared to be predicted. However, differences between appropriate predicted morphologies (for example, between negative and neutral potential cells at high cell pH) were not statistically significant in this data set ($p > 0.10$).

Adjusted-*y* plots

Using predictions of the mathematical model, an adjusted morphological index was computed as a function of each of the three modeled variables (Fig. 5). An adjusted-*y* plot of a multivariate dataset presents the *y* variable as a function of one of the *x* variables, after adjusting for effects of other *x* variables (BBN Software Products Corporation, 1988). This analytical tool allowed visualization of the individual predicted influences of cell pH, membrane potential, and cell water on red cell morphology in this data set. The plots also displayed the amount of variability remaining in the data set after predicted effects were accounted for.

Consistent with stratification and significance testing, the adjusted morphology plots showed cell pH to have the greatest overall influence in the data set. The adjusted morphological index varied +2.2 units (from −0.7 to +1.5) over the cell pH range 5.5–9.0 (Fig. 5 *A*). In contrast, adjusted morphology varied just −0.6 units over the full membrane potential range (Fig. 5 *B*) and −0.7 units over the full cell water range (Fig. 5 *C*).

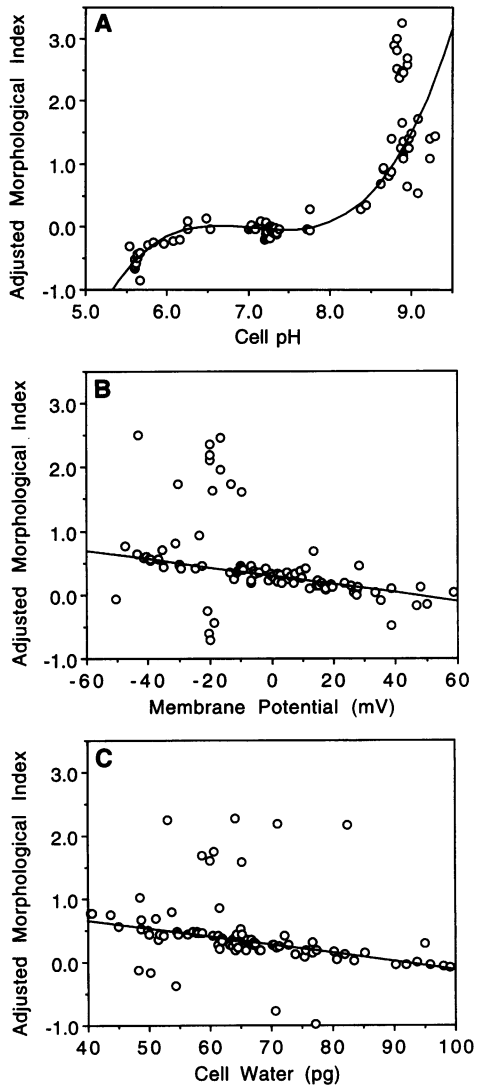

FIGURE 5 Predictions of the model: separate effects of cell pH, membrane potential, and cell water on calculated red cell morphology. Adjusted-*y* plots consisting of adjusted morphological index for each case and an adjusted fit function were constructed as described (BBN Software Products Corporation, 1988) with respect to the predictors cell pH (*A*), membrane potential (*B*), and cell water (*C*).

TABLE 3 Model of morphological index as a function of cell pH, membrane potential, and cell water*

Factor#	Coefficient	Standard error	*t* value
1	−0.035	0.018	−1.90
pH	−0.093	0.070	−1.33
pH^2	0.079	0.022	3.56
pH^3	0.225	0.033	6.81
pH*pot	0.0083	0.0026	3.24
pH^2*pot	−0.0044	0.0009	−4.78
pH^3*pot	−0.0028	0.0013	−2.24
pH*cw	−0.0082	0.0019	−4.27
pH^2*cw	−0.0077	0.0013	−6.13

*Condition # = 9.8, R^2_{adj} = 0.909, RMS error = 0.141.
#pH = (cell pH − 7.2); *cw* = (cell water (pg) − 67); pot = potential (mV).

The adjusted-*y* plots also showed that some data set variability still remained after modeled effects of cell pH, membrane potential, and cell water were accounted for: 10 or more of the 89 plotted points lie relatively distant from the adjusted morphological index curves. Fig. 5 *A* shows that this unmodeled variability occurred exclusively at high cell pH. The source of this residual variability is unclear. The morphology of high pH cells may be particularly sensitive to minor variations in conditions occurring among experiments performed on different days, or to variations among cells from different donors. There could be an unmodeled physiological variable that affects the morphology only of high pH cells. For example, although alteration of cell chloride does not independently affect shape (see above), cell chloride or other components of cell ionic

strength might have secondary morphological effects at high cell pH.

Effect of cell water variation on the morphology of high pH cells in individual experiments

Although the mathematical model did not predict a significant morphological influence for cell water at any pH, it suggested such an effect at high cell pH. Moreover, there is precedence in the red cell literature for the morphological effects of cell shrinkage (see Discussion). To test more directly the possibility that cell water modulates the extent of echinocytosis of high pH cells, individual experiments were examined. The data set contained six experiments in which the cell water of high pH cells varied. The two experiments in which cells were near neutral membrane potential are shown in Fig. 6. In both of these experiments, morphological index was significantly greater in shrunken cells than in cells with a normal range of cell water ($p < 0.01$, *open circles*, or $p < 0.05$, *closed circles*, one-tailed t-test), and was significantly less in swollen cells than in normal cell water cells ($p < 0.01$, one-tailed t-test, both experiments). Of the other four experiments, two were at negative and two were at positive membrane potential (Table 4). In all of these experiments, the values of morphological index decreased as cell water increased, but the effects were significant in only two experiments. Thus the data show a consistent modulatory effect of cell water on the echinocytosis of high pH cells, with shrinkage intensifying crenation and swelling relieving it. However, both the extent of the modulatory effect and the degree of high pH echinocytosis vary widely among experiments.

TABLE 4 Effect of variation of cell water on morphology of high pH cells

Experiment	Cell pH*	Membrane potential (mV)	Cell water (pg)	Morphological index
1	8.8 ± 0.1	−19 ± 2	53 ± 0	3.42 ± 0.07
			64 ± 2	3.22 ± 0.20
			82 ± 0	2.82 ± 0.01
2	9.2 ± 0.1	−20 ± 1	54 ± 0	2.44 ± 0.16#
			71 ± 1	1.30 ± 0.25
3	8.7 ± 0.0	+20 ± 5	54 ± 0	0.08 ± 0.04
			66 ± 1	−0.02 ± 0.03
			90 ± 1	−0.06 ± 0.05
4	9.0 ± 0.1	+18 ± 5	49 ± 0	2.07 ± 0.02#
			65 ± 1	1.01 ± 0.24
			94 ± 1	0.04 ± 0.06§

*Cell pH and membrane potential values are averaged over the samples in each experiment.
#Significantly greater than morphological index of normal cell water sample ($p < 0.05$, one-tailed t-test).
§Significantly less than morphological index of normal cell water sample ($p < 0.05$, one-tailed t-test).

DISCUSSION

Understanding of the human erythrocyte shape change that occurs in altered external pH would provide insight into how cell physiological properties affect membrane structure. In the present study, physiological mediators of this shape change were investigated by examining the morphology of cells in a wide range of physiological states. As in the companion study (Gedde and Huestis, 1997), membrane potential did not independently affect red cell shape. In addition, cell water and cell chloride concentration did not independently affect shape. In contrast, change in cell pH was both necessary and sufficient for erythrocyte shape change in this experimental system. Shape dependence on pH was strikingly nonlinear, with stomatocytosis below cell pH 6.3, echinocytosis above cell pH 7.9, and a plateau region of normal discoid morphology between these limits. (This result also has been demonstrated directly by equilibrating red cells in buffers designed to vary cell pH but maintain membrane potential and cell water within normal ranges (Gedde et al., 1995).) The possibility of secondary, pH-dependent shape effects of membrane potential and cell water was also examined. The present data suggested, but did not prove, that membrane potential modulated the shapes of low and high pH cells. In contrast, cell water modulation of high pH echinocytosis was statistically significant in several experiments in the present data set.

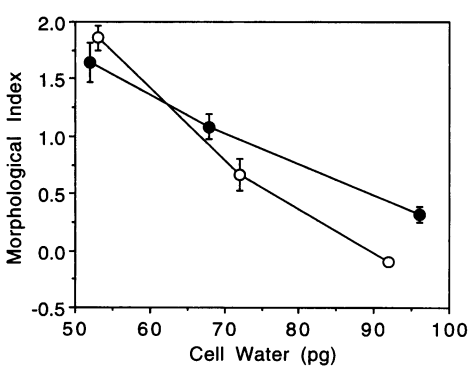

FIGURE 6 Effect of cell water on morphology of cells at high pH and neutral membrane potential. The two data set experiments in which cell water varied at high cell pH and approximately neutral membrane potential are shown. The cell state was varied by the buffer variation method (Materials and Methods). Cell pHs were 8.7 ± 0.1 (○) and 8.9 ± 0.1 (●). Membrane potentials were +12 ± 5 mV (○) and −6 ± 1 mV (●). Morphologies of shrunken and swollen cells in the individual experiments were significantly different from those of normal cell water cells, as detailed in the Results.

These results show that cell pH, a fundamental biological property, independently modulates erythrocyte membrane structure. In general, distinctive features of cell pH-mediated shape changes are that they proceed at ambient temperature, they can occur within seconds, and they reverse upon normalization of the extracellular environment. Thus irreversible denaturations, energy-dependent steps, or disruption of high-affinity protein-protein bonds are unlikely to be involved in these transitions. Rather, they appear to involve subtle shifts in low-affinity molecular interactions, such as might result from pH titration of membrane components.

Nonlinearity of shape dependence on cell pH

Any proposed mechanism of this shape change should account for its strikingly nonlinear (third-order) dependence on cell pH (Fig. 5 *A*; Gedde et al., 1995). This dependence is consistent with several mechanistic possibilities. First, low pH stomatocytosis and high pH echinocytosis could result from two independent critical events, one occurring below about cell pH 6.5, the other above about cell pH 8.0. Second, both shape changes could result from titration of a single membrane structure; to produce the observed shape dependence on pH, the hypothetical structure would have to have a complex, cooperative pH titration curve, perhaps similar to that demonstrated for hemoglobin (Huestis and Raftery, 1972). A third possibility is that a single, relatively simple titration causes shape changes at both low and high pH, and this process is opposed in the neutral pH range by titration of a second structure with an opposite shape effect. This third scenario is particularly intriguing in light of the predicted and observed pH-dependent influence of spectrin on shapes of isolated erythrocyte membranes (below).

Candidate structures for mediation of cell pH-dependent shape change

Spectrin, the major protein in the erythrocyte membrane skeleton, would seem to be a likely candidate for the membrane component mediating cell pH-dependent shape change. Charge on spectrin changes markedly between pH 5.5 and 9.0 (isoelectric point 4.8; Elgsaeter et al., 1976). Moreover, the ionic gel model of the erythrocyte membrane skeleton (Stokke et al., 1986) proposes that spectrin titration causes expansion and contraction of the membrane skeleton: as the spectrin net charge increases or decreases, the number of counterions required for electroneutrality within the membrane skeleton is expected to increase or decrease. Additional counterions, as would be present at high pH, would increase membrane skeleton osmotic potential, causing it to hold larger amounts of water and expand; at low pH, loss of counterions would cause the membrane skeleton to contract.

The usefulness of the ionic gel model is demonstrated by observations of isolated erythrocyte membranes (ghosts). These preparations contract in low pH or moderate ionic strength solutions, and expand in high pH or very low ionic strength solutions (Johnson et al., 1980; Lange et al., 1982; Nakao et al., 1987). The spectrin volume changes cause the membranes to become echinocytic at low pH and stomatocytic at high pH, as predicted by the ionic gel model (Elgsaeter et al., 1986), but in direct contrast to the shape behavior of intact cells. Therefore, pH titration of the membrane skeleton does not explain cell pH-mediated shape change; moreover, a plausible mechanism for this shape change should take into account the opposing pH-dependent effects of spectrin.

Intramembrane particle aggregation in human erythrocyte ghosts (Pinto da Silva, 1972; Elgsaeter and Branton, 1974; Elgsaeter et al., 1976) is another reversible, pH-dependent process that could be relevant to the present observations. In freeze-fracture preparations, the transmembrane particles of erythrocyte ghosts (now known to be band 3, the erythrocyte anion exchanger) were observed to be disaggregated at neutral and alkaline pH, but to rapidly and reversibly aggregate at pH 5.5. However, this process has not been observed to occur in conditions comparable to those in intact cells. In the initial report, all solutions contained 1 mM calcium chloride; moreover, although particle aggregation was observed at pH 5.5 in hypotonic conditions, particles remained disaggregated at pH 5.5 when 0.15 M sodium chloride was present (Pinto da Silva, 1972). In another report, pH 5.5 particle aggregation was observed only subsequent to pretreatments that removed most of the spectrin-based membrane skeleton, whether conditions were hypotonic or isotonic (Elgsaeter and Branton, 1974). Thus the observations on reversible, pH-dependent transmembrane particle aggregation do not appear relevant to the pH-dependent shape changes of intact cells.

Another possibility is that pH-dependent shape changes are mediated by phospholipid species present in the erythrocyte inner membrane and titrating in the appropriate pH range (phosphatidylinositol-4-phosphate, phosphatidylinositol-4,5-bisphosphate, and phosphatidic acid; phosphate pK_2 6 to 8; Tocanne and Teissie, 1990). However, we have demonstrated that cell pH-mediated shape changes remain intact in cells depleted of these pH-titratable lipids (Gedde et al., 1995).

Although other cell components titrate in the relevant pH range (for example, the isoelectric point of hemoglobin is 6.8; Antonini and Brunori, 1975), there are currently no data to implicate any known cell or membrane component in the mechanism of cell pH-mediated shape change.

Despite the lack of a molecular mechanism, it is reasonable to consider what might be the mechanical basis of the membrane curvature changes seen in altered-pH erythrocytes. The weight of current evidence supports layer coupling, first articulated as the bilayer couple hypothesis (Sheetz and Singer, 1974), as the general mechanism of erythrocyte shape change (Elgsaeter et al., 1986; Bull and Brailsford, 1989; Steck, 1989). The erythrocyte membrane is composed of several tightly associated layers: two lipid leaflets, the inner surface membrane skeleton, and the outer surface glycocalyx. Physical and chemical treatments cause individual layers to increase or decrease in area. Because the layers are coupled, change in area of one layer relative to others induces a deformable membrane to bend. For example, an increase in area of the outer lipid leaflet would effect positive curvature (echinocytosis), and a decrease in area of the elastic membrane skeleton would have the same effect.

Although the basic premise of layer coupling models, that change in membrane curvature corresponds to change in area of a membrane layer, has been questioned (Bull and Brailsford, 1989), both mathematical and biochemical evidence that echinocytes have expanded outer monolayers has been provided (Ferrell et al., 1985). Spin-labeling and ra-

diolabeling data showed that incorporation of 4×10^6 molecules of exogenous phosphatidylcholine per cell, estimated to expand the red cell membrane outer monolayer by 1.7%, converts discocytes to stage 3 echinocytes. Geometrical modeling of discocytes and stage 3 echinocytes yielded a calculated inner/outer monolayer surface area difference of 0.7%. This work gave the bilayer couple hypothesis a quantitative basis and demonstrated that it can explain erythrocyte shape changes without the need to hypothesize rearrangement of the membrane skeleton or of other structures.

In this context, it is interesting to note that several peripheral and cytoplasmic erythrocyte proteins have been shown to insert hydrophobically and in a pH-dependent manner into anionic lipid-containing model membranes. These proteins include spectrin (Mombers et al., 1980), hemoglobin (Shviro et al., 1982; Szebeni et al., 1988), band 4.1 (Schiffer et al., 1988), and actin (St-Onge and Gicquaud, 1990). It is interesting to speculate that increased insertion of a cell protein into the red cell inner leaflet at low pH, either electrostatically between lipid headgroups or hydrophobically between lipid hydrocarbon chains, could cause an increase in the inner monolayer surface area and result in low cell pH stomatocytosis. Reduction of such interactions at high pH could be the cause of high cell pH echinocytosis. Superposition of these putative protein-membrane interactions on the opposing effects of pH-dependent spectrin contraction and expansion might explain the strikingly nonlinear pH dependence of erythrocyte shape.

Dependence of shape on cell water

This study has shown that cell water does not independently affect erythrocyte shape (see also Gedde at al., 1995). This finding was unexpected: shrinkage-associated crenation is a classical observation (for example, Rand and Burton, 1964); in addition, the preceding study (Gedde and Huestis, 1997) demonstrated that shrinkage can result in echinocytosis (Fig. 7), and the present study has shown that shrinkage of high pH cells intensifies high pH echinocytosis (Fig. 6).

From a membrane mechanical perspective, cell water content is expected to affect cell shape through its effects on cell deformability, because the cell surface area-to-volume ratio (SA:V) restricts the range of geometrically allowed shapes (Mohandas et al., 1983; Svetina and Zeks, 1989). At maximum cell water, when SA:V is at a minimum, the only allowed shape is a sphere. As the cell shrinks, SA:V increases, and more shapes are permitted. This covariance of cell water content and cell deformability appears to explain the modulation of high cell pH echinocytosis reported in the present study. A swollen high pH cell would be less deformable than one with normal water content, so the most strongly crenated shapes would be disallowed. Conversely, a high pH cell that is shrunken would have an increased cell deformability, allowing a degree of echinocytosis not otherwise permitted.

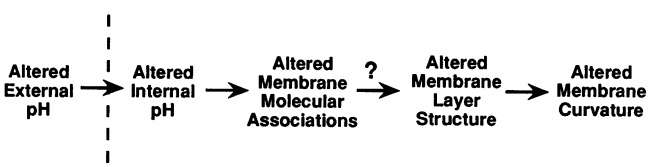

FIGURE 7 Possible chain of causation of erythrocyte shape change in altered external pH.

This relationship between cell water content and deformability may also explain reports of red cells crenated in hypertonic saline. In one authoritative study, drops of whole blood were mixed with several volumes of saline on glass slides (Rand and Burton, 1964). When washed red cells are placed on glass, they become echinocytic (glass crenation) (Furchgott and Ponder, 1940), but the albumin in whole blood stabilizes the cells against this shape change (Furchgott and Ponder, 1940; Bull and Brailsford, 1989). High cell pH echinocytosis and glass crenation appear to be related, because an increase in pH of solutions in contact with glass is required for glass crenation (Trotter, 1956; Weed and Chailley, 1973). Therefore, it seems plausible that when whole blood is mixed with saline on glass slides, as in the experiment described above, red cell cytoplasmic pH becomes elevated. In that experiment, cells mixed with isotonic saline had a normal biconcave shape, but cells mixed with hypertonic saline were shrunken and crenated. This "hypertonic crenation" may represent glass crenation that in normally hydrated cells was prevented by albumin binding, but which became manifest as the cells were made more deformable by shrinkage. This same process appears to pertain to shrinkage-associated crenation of cells at normal external pH and positive membrane potential (figure 7 in Gedde and Huestis, 1997). These cells are expected to have slightly elevated cytoplasmic pH (to pH 7.7 or 7.8), which is expected to confer an echinocytic tendency. Shrinkage under these conditions apparently allowed the crenation to develop.

Model chain of causation

The chain of causation between changed external pH and changed shape may involve the steps in Fig. 7. First, changed external pH alters cytoplasmic pH according to cell physiological principles. Second, the altered cell pH perturbs noncovalent molecular associations in the membrane, either by destabilizing existing associations or stabilizing new ones. Third, in a deformable membrane, the changed pattern of forces may mandate the contraction or expansion of a membrane layer. Fourth, this produces altered membrane curvature and shape. Some of the molecular membrane associations involved apparently are present only in intact cells, and not in membranes that have been subjected to hypotonic lysis.

Significance

Cell pH has been shown to have a regulatory role in the metabolism and development of certain organisms (review: Busa and Nuccitelli, 1984), and there is increasing evidence that cell pH is involved in the modulation of cytoskeletal interactions (Busa, 1986). However, difficulty in measuring intracellular pH in most cells has impeded the understanding of its role in cell biological processes. As shown here, the mature erythrocyte's intracellular pH is readily manipulated and measured; thus the red cell is a useful model for studying responses of biological membranes to changes in intracellular pH. Elucidation of pH-dependent events in the erythrocyte membrane could provide basic information applicable to other biological membranes.

We gratefully acknowledge the assistance of Dr. Andrew Cucciara, General Research Center, University of Pennsylvania, with statistical portions of the manuscript.

REFERENCES

Antonini, E., and M. Brunori. 1975. Hemoglobin and methemoglobin. *In* The Red Blood Cell. D. M. Surgenor, editor. Academic Press, New York. 753–797.

BBN Software Products Corporation. 1988. RS/Explore Statistical Appendices. Cambridge, MA.

Bernhardt, I., E. Donath, and R. Glaser. 1984. Influence of surface charge and transmembrane potential on rubidium-86 efflux of human red blood cells. *J. Membr. Biol.* 78:249–255.

Bernhardt, I., A. Erdmann, R. Vogel, and R. Glaser. 1987. Factors involved in the increase of K^+ efflux of erythrocytes in low chloride media. *Biomed. Biochim. Acta.* 46:S36–S40.

Bessis, M., and M. Prenant. 1972. Topographie de l'apparition des spicules dans les erythrocytes creneles (echinocytes). *Nouv. Rev. Fr. Hematol.* 12:351–364.

Bull, B. S., and D. Brailsford. 1989. Red blood cell shape. *In* Red Blood Cell Membranes: Structure, Function, Clinical Implications. P. Agre and J. C. Parker, editors. M. Dekker, New York. 401–421.

Busa, W. B. 1986. Mechanisms and consequences of pH-mediated cell regulation. *Annu. Rev. Physiol.* 48:389–402.

Busa, W. B., and R. Nuccitelli. 1984. Metabolic regulation via intracellular pH. *Am. J. Physiol.* 246:R409–R438.

Donlon, J. A., and A. Rothstein. 1969. The cation permeability of erythrocytes in low ionic strength media of various tonicities. *J. Membr. Biol.* 1:37–52.

Elgsaeter, A., and D. Branton. 1974. Intramembrane particle aggregation in erythrocyte ghosts. I. The effects of protein removal. *J. Cell Biol.* 63:1018–1030.

Elgsaeter, A., D. M. Shotton, and D. Branton. 1976. Intramembrane particle aggregation in erythrocyte ghosts. II. The influence of spectrin aggregation. *Biochim. Biophys. Acta.* 426:101–122.

Elgsaeter, A., B. T. Stokke, A. Mikkelsen, and D. Branton. 1986. The molecular basis of erythrocyte shape. *Science.* 234:1217–1223.

Ferrell, J. E., Jr., K.-J. Lee, and W. H. Huestis. 1985. Membrane bilayer balance and erythrocyte shape: a quantitative assessment. *Biochemistry.* 24:2849–2857.

Freedman, J. C., and J. F. Hoffman. 1979. Ionic and osmotic equilibria of human red blood cells treated with nystatin. *J. Gen. Physiol.* 74:157–185.

Furchgott, R. F., and E. Ponder. 1940. Disk-sphere transformation in mammalian red cells. II. The nature of the anti-sphering factor. *J. Exp. Biol.* 17:117–127.

Gedde, M. M., and W. H. Huestis. 1997. Membrane potential and human erythrocyte shape. *Biophys. J.* 72:000–000.

Gedde, M. M., E. Yang, and W. H. Huestis. 1995. Shape response of human erythrocytes to altered cell pH. *Blood.* 86:1595–1599.

Glaser, R. 1979. The shape of red blood cells as a function of membrane potential and temperature. *J. Membr. Biol.* 51:217–228.

Hennekens, C. H., and J. E. Buring. 1987. Epidemiology in Medicine. Little, Brown and Company, Boston.

Herrmann, A., and P. Muller. 1986. Ionic-strength dependent alterations of membrane structure of red blood cells. *Biosci. Rep.* 6:1007–1015.

Huestis, W. H., and M. A. Raftery. 1972. Observation of cooperative ionizations in hemoglobin. *Proc. Natl. Acad. Sci. USA.* 69:1887–1891.

Jacobs, M. H., and D. R. Stewart. 1947. Osmotic properties of the erythrocyte. XII. Ionic and osmotic equilibria with a complex external solution. *J. Cell. Comp. Physiol.* 30:79–103.

Johnson, R. M., G. Taylor, and D. B. Meyer. 1980. Shape and volume changes in erythrocyte ghosts and spectrin-actin networks. *J. Cell Biol.* 86:371–376.

Jones, G. S., and P. Knauf. 1985. Mechanism of the increase in cation permeability of human erythrocytes in low-chloride media: involvement of the anion transport protein capnophorin. *J. Gen. Physiol.* 86:721–738.

Lange, Y., R. A. Hadesman, and T. L. Steck. 1982. Role of the reticulum in the stability and shape of the isolated human erythrocyte membrane. *J. Cell Biol.* 92:714–721.

Mohandas, N., J. A. Chasis, and S. B. Shohet. 1983. The influence of membrane skeleton on red cell deformability, membrane material properties, and shape. *Semin. Hematol.* 20:225–242.

Mombers, C., J. De Gier, R. A. Demel, and L. L. M. Van Deenan. 1980. Spectrin-phospholipid interaction: a monolayer study. *Biochim. Biophys. Acta.* 603:52–62.

Nakao, M., Y. Jinbu, S. Sato, Y. Ishigami, T. Nakao, E. Ito-Ueno, and K. Wake. 1987. Structure and function of red cell cytoskeleton. *Biomed. Biochim. Acta.* 46:S5–S9.

Pinto da Silva, P. 1972. Translational mobility of the membrane intercalated particles of human erythrocyte ghosts. *J. Cell Biol.* 53:777–787.

Rand, R. P., and A. C. Burton. 1964. Mechanical properties of the red cell membrane. I. Membrane stiffness and intracellular pressure. *Biophys. J.* 4:115–135.

Rand, R. P., A. C. Burton, and P. Canham. 1965. Reversible changes in shape of red cells in electrical fields. *Nature.* 205:977–978.

Schiffer, K. A., J. Goerke, N. Duzgunes, J. Fedor, and S. B. Shohet. 1988. Interaction of erythrocyte protein 4.1 with phospholipids. A monolayer and liposome study. *Biochim. Biophys. Acta.* 937:269–280.

Sheetz, M. P., and S. J. Singer. 1974. Biological membranes as bilayer couples: a molecular mechanism of drug-erythrocyte interactions. *Proc. Natl. Acad. Sci. USA.* 71:4457–4461.

Shviro, Y., I. Zilber, and N. Shaklai. 1982. The interaction of hemoglobin with phosphatidylserine vesicles. *Biochim. Biophys. Acta.* 687:63–70.

Steck, T. L. 1989. Red cell shape. *In* Cell Shape: Determinants, Regulation, and Regulatory Role. W. D. Stein and F. Bronner, editors. Academic Press, San Diego. 205–245.

Stokke, B. T., A. Mikkelsen, and A. Elgsaeter. 1986. Spectrin, human erythrocyte shapes, and mechanochemical properties. *Biophys. J.* 49: 319–327.

St-Onge, D., and C. Gicquaud. 1990. Research on the mechanism of interaction between actin and membrane lipids. *Biochem. Biophys. Res. Commun.* 167:40–47.

Svetina, S., and B. Zeks. 1989. Membrane bending energy and shape determination of phospholipid vesicles and red blood cells. *Eur. Biophys. J.* 17:101–111.

Szebeni, J., H. Hauser, C. D. Eskelson, R. R. Watson, and K. H. Winterhaltar. 1988. Interaction of hemoglobin derivatives with liposomes. Membrane cholesterol protects against the changes of hemoglobin. *Biochemistry.* 27:6425–6434.

Tocanne, J.-F., and J. Teissie. 1990. Ionization of phospholipids and phospholipid-supported interfacial lateral diffusion of protons in membrane model systems. *Biochim. Biophys. Acta.* 1031:111–142.

Trotter, W. D. 1956. The slide-coverslip disc-sphere transformation in mammalian erythrocytes. *Br. J. Haematol.* 2:65–74.

Weed, R. I., and B. Chailley. 1973. Calcium-pH interactions in the production of shape change in erythrocytes. *In* Red Cell Shape: Physiology, Pathology, Ultrastructure. M. Bessis, R. I. Weed and P. F. Leblond, editors. Springer-Verlag, New York. 55–68.